

**Internal decay of the ( $10^-$ ) intruder state in  $^{184}\text{Tl}$** 

C. Van Beveren,<sup>1,\*</sup> A. N. Andreyev,<sup>2,3</sup> A. E. Barzakh,<sup>4</sup> T. E. Cocolios,<sup>5,6</sup> D. Fedorov,<sup>4</sup> V. N. Fedosseev,<sup>7</sup> R. Ferrer,<sup>1</sup> M. Huyse,<sup>1</sup> U. Köster,<sup>8</sup> J. Lane,<sup>9</sup> V. Liberati,<sup>9</sup> K. M. Lynch,<sup>5,6</sup> B. A. Marsh,<sup>5</sup> T. J. Procter,<sup>6</sup> D. Radulov,<sup>1</sup> E. Rapisarda,<sup>5,1</sup> K. Sandhu,<sup>9</sup> M. D. Seliverstov,<sup>2,4,5,10</sup> P. Van Duppen,<sup>1</sup> M. Venhart,<sup>11</sup> and M. Veselsky<sup>11</sup>

<sup>1</sup>*KU Leuven, Instituut voor Kern- en Stralingsfysica, B-3001 Leuven, Belgium*

<sup>2</sup>*Department of Physics, University of York, York YO10 5DD, United Kingdom*

<sup>3</sup>*Advanced Science Research Center (ASRC), Tokai-mura, Japan*

<sup>4</sup>*Petersburg Nuclear Physics Institute, NRC Kurchatov Institute, 188300 Gatchina, Russia*

<sup>5</sup>*ISOLDE, CERN, CH-1211 Geneve 23, Switzerland*

<sup>6</sup>*University of Manchester, Manchester, United Kingdom*

<sup>7</sup>*EN Department, CERN, CH-1211 Geneve 23, Switzerland*

<sup>8</sup>*Institut Laue Langevin, 6 rue Jules Horowitz, F-38042 Grenoble Cedex 9, France*

<sup>9</sup>*UWS, University of the West of Scotland, Paisley, United Kingdom*

<sup>10</sup>*School of Engineering and Science, University of the West of Scotland, Paisley PA1 2BE, United Kingdom*

<sup>11</sup>*Institute of Physics, Slovak Academy of Sciences, 845 11 Bratislava, Slovakia*

(Received 16 June 2015; published 30 July 2015)

Decay spectroscopy of  $^{184}\text{Tl}$  has been performed at the CERN Isotope Separator On-Line (ISOLDE) facility. An excitation energy of 506.1(1) keV and a half-life of 47.1(7) ms of the intruder based ( $10^-$ ) state have been extracted. The internal decay characteristics of this state are determined and discussed, extending the systematics of such states in the even-mass thallium nuclei below neutron midshell at  $N = 104$ . The retardation factors of the isomeric  $M2$  and  $E3$  transitions are deduced and compared with retardation factors in neighboring odd-mass and even-mass thallium isotopes. The new information is combined with a review of hindered and unhindered  $\alpha$ -decay data of  $^{187-192}\text{Bi}$  populating levels in daughter nuclei  $^{183-188}\text{Tl}$  and supports the interpretation of the intruder character of the ( $10^-$ ) state in  $^{184}\text{Tl}$ .

DOI: [10.1103/PhysRevC.92.014325](https://doi.org/10.1103/PhysRevC.92.014325)

PACS number(s): 21.10.-k, 23.20.Lv, 27.70.+q, 29.38.-c

**I. INTRODUCTION**

The neutron-deficient thallium isotopes with one proton less than the  $Z = 82$  shell closure, represent an interesting region of the nuclear chart to study in detail shape coexistence [1–3] in nuclei, i.e., the existence of states with different shapes at low excitation energy in the same atomic nucleus. Extensive investigation of this phenomenon for the lead region together with a substantial development of new theoretical approaches constitutes the basis to further extend the experimental research to the neutron-deficient thallium isotopic chain. For an overview on the experimental evidence and the recent progress in theoretical descriptions, we refer to [4].

In the neutron-deficient, odd-mass thallium nuclei, states with different shapes, whose structure has been linked to specific proton orbitals above and below  $Z = 82$ , are present at low energy. Next to spherical proton-hole configurations, involving the “normal”  $\pi 3s_{1/2}$  and  $\pi 2d_{3/2}$  orbitals, one particle-two hole (1p-2h) configurations, involving the  $\pi 1h_{9/2}$  and  $\pi 1i_{13/2}$  orbitals from above the  $Z = 82$  shell closure, that lead to deformation, are identified. Rotational band structures built on top of the latter, so-called intruder states, were

observed (see Fig. 18 in Ref. [4]). The energy of the 1p-2h band heads show typical parabolic behavior as a function of neutron number, reaching a minimum at  $N = 108$ , close to  $N = 104$ , midshell between  $N = 82$  and  $N = 126$ . This leads for the case of the ( $9/2^-$ ) state to isomerism. For  $^{185,191,193,195,197}\text{Tl}$ , the mean-square charge radii of the ( $1/2^+$ ) ground state as well as the ( $9/2^-$ ) isomer were measured. A large isomer shift was observed, implying a larger deformation of the ( $9/2^-$ ) isomer relative to that of the ( $1/2^+$ ) ground state [5].

The well-established occurrence of intruder states and shape coexistence in odd-mass thallium isotopes, raises the question of where such states appear in the even-mass thallium isotopes, especially in the lightest isotopes below  $N = 104$ , and what role the unpaired neutron plays when coupled to the unpaired proton. The coupling of this unpaired neutron and unpaired proton (normal as well as intruder) results in multiplets of states from which some members can become isomeric. This is further complicated by a relatively small energy spacing between these multiplet states and/or the collective bands built on top of the intruder configurations (see, e.g., [6]). This results in complex decay schemes and low-energy, highly converted transitions must be reliably identified and located in the decay schemes.

However, by focusing on isomeric  $\gamma$  radiation and/or by using the selectivity of the  $\alpha$ -decay process, the position of the intruder ( $8,9,10^-$ ) state, originating from the  $[\pi 1h_{9/2} \otimes \nu 1i_{13/2}]$  coupling, relative to the normal ( $7^+$ ) state, originating from the  $[\pi 3s_{1/2} \otimes \nu 1i_{13/2}]$  coupling, could be measured in a number of thallium isotopes. Also here the energy difference

\*celine.vanbeveren@fys.kuleuven.be

between the intruder and normal configuration exhibits a parabolic behavior; similar to the one observed in the odd-mass thallium nuclei (see Fig. 7b in Ref. [7]). It was also found that in the odd-mass as well as the even-mass thallium isotopes, the internal transition (IT) of the intruder isomer is hindered, another fingerprint of shape coexistence [1].

In this paper we focus on the IT of the  $(10^-)$  state in  $^{184}\text{Tl}$ . Prior to our study, the location of this isomeric  $(10^-)$  state was found at 500(5) keV above the  $\beta$ -decaying  $(7^+)$  state, determined through the  $\alpha$  decay of  $^{188}\text{Bi}$ , but its half-life and decay characteristics were unknown [8]. The presumed  $(10^-)[\pi 1h_{9/2} \otimes \nu 1i_{13/2}]$  state in  $^{188m1}\text{Bi}$  decays by unhindered  $\alpha$  decay to the  $(10^-)$  state, explained as the  $[\pi 1h_{9/2} \otimes \nu 1i_{13/2}]$  intruder state in  $^{184}\text{Tl}$ , and by a strongly hindered decay to the  $(7^+)$  state, explained as the normal  $[\pi 3s_{1/2} \otimes \nu 1i_{13/2}]$  state in  $^{184}\text{Tl}$ . The  $(3^+)[\pi 1h_{9/2} \otimes \nu 3p_{3/2}]$  state  $^{188m2}\text{Bi}$  decays unhindered to a  $(3^+)$  state, explained as the  $[\pi 1h_{9/2} \otimes \nu 3p_{3/2}]$  intruder state, 99 keV above the weakly fed  $(2^-)$   $\beta$ -decaying state, explained as the normal  $[\pi 3s_{1/2} \otimes \nu 3p_{3/2}]$  state. As the relative position of the  $\alpha$ -decaying states in  $^{188}\text{Bi}$  is unknown, the relative position of the  $(7^+)$  and  $(2^-)$   $^{184}\text{Tl}$   $\beta$ -decaying states is not fixed [8]. Direct mass measurements in a Penning trap could not resolve this [9].

In our study, combining the high selectivity of the Resonant Ionization Laser Ion Source (RILIS) [10–12] with decay spectroscopy and the in-source laser spectroscopy method [13–15], exotic thallium isotopes down to  $N = 97$  have been studied at the Isotope Separator On-Line Device ISOLDE [16] CERN, Geneva, Switzerland, using the Windmill detection system [17–19]. Complementary decay data on isomerically purified sources were collected. This has led to the characterization of the decay of the  $(10^-)$ ,  $(2^-)$ , and  $(7^+)$  states in  $^{184}\text{Tl}$ . In the present study, the IT characteristics of the  $(10^-)$  intruder state are presented and discussed. The results of the  $\beta^+/\text{EC}$  decay of the  $(7^+)$  and  $(2^-)$  states as well as the  $\alpha$  decay of the three long living states will be reported elsewhere, respectively [20,21].

## II. EXPERIMENTAL SETUP

The experiment was carried out at the CERN Isotope Separator On-Line Device (ISOLDE) facility [16]. Protons from the CERN Proton Synchrotron Booster, with an energy of 1.4 GeV and an intensity up to 2.1  $\mu\text{A}$ , impinged on a 50 g/cm<sup>2</sup> UC<sub>x</sub> target. The proton beam consisted of a repeated sequence of pulses (typically 35–40) separated by periods of 1.2 s, called a supercycle. The radioactive thallium isotopes were predominantly formed through proton-induced spallation. After proton impact, recoiling nuclei stopped in the target matrix, diffused out and effused towards the hot cavity kept at a high temperature of  $\sim 2300$  K. In the hot cavity thallium isotopes were selectively laser-ionized using the same scheme as in the study of [18]. The excitation from the atomic ground state to an intermediate electronic state  $6d^2D_{3/2}$  ( $36117.9\text{ cm}^{-1}$ ) was performed by a frequency-doubled narrow-band tunable dye laser beam at 276.79 nm with a linewidth of 0.8 GHz. The subsequent ionization of excited thallium atoms was accomplished by a powerful 532 nm beam of 10 kHz EdgeWave Nd:YAG laser, that was also used as a pump source for the first excitation step laser (for details

of RILIS laser setup see [11]). The nonselective thermal ionization of thallium on a surface of the hot cavity was also present, however it was approximately 20 times less efficient than the laser ionization. The ions were then accelerated to an energy of 30 keV and separated according to their mass to charge ratio by the ISOLDE General Purpose Separator. As a result, a high-purity beam of  $^{184}\text{Tl}$  was obtained. Moreover, by tuning the first excitation step frequency of the laser to selectively enhance the production of the  $(10^-)$  state, an isometrically purified beam was produced. This was possible due to the marked difference in hyperfine structures of the different  $^{184}\text{Tl}$  isomers. After separation, the ion beam entered the Windmill system [17–19] through a collimator and was then implanted in one out of the ten carbon foils (6 mm diameter, 20  $\mu\text{g}/\text{cm}^2$  thickness [22]) that were mounted on a rotating wheel. After each supercycle the wheel was rotated to move away the radioactivity from the implantation position and present a fresh foil in front of the ion beam. The separator beam gate was opened for different periods during the experimental campaign varying between 14 and 300 ms after the proton pulse in order to limit the amount of activity implanted on the foil.

One Si detector (Si1: total area 450 mm<sup>2</sup>, 300  $\mu\text{m}$  depletion depth) was placed upstream 7 mm away from the implantation foil. The beam passed through a hole of 8 mm diameter. The other Si detector (Si2: total area 300 mm<sup>2</sup>, 500  $\mu\text{m}$  depletion depth) was placed 4 mm behind the implantation foil. These detectors were also used for detecting  $\beta^+$  particles and conversion electrons (CE). The detection efficiency of Si2 for electrons was determined by using the CE from the 375 keV E0 transition ( $0_2^+ \rightarrow 0_1^+$ ) in  $^{184}\text{Hg}$ , where the former is populated in the  $\beta^+/\text{EC}$  decay of  $^{184}\text{Tl}$ . Due to the limited resolution of the Si2 detector,  $M$  (and higher order)-CE could not be resolved from  $L$ -CE. This results in 7.6(16)% at 292 keV ( $K$  conversion) and 7.2(17)% at 360 keV ( $L, M$  conversion) (see [20]). The two Si detectors were placed at the implantation position in close geometry, covering a total solid angle of 51% of  $4\pi$ . To detect  $\gamma$  rays two single crystal HPGe detectors were placed outside the vacuum chamber at 0° (Ge1) and 90° (Ge2), respectively, with respect to the direction of the incoming beam. The typical energy resolution (full width half-maximum) of each crystal for 1.3 MeV  $\gamma$  radiation was  $\sim 3.1$  keV. The absolute photopeak efficiency for the 506 keV line, the strongest transition in the IT decay of the  $(10^-)$  state in  $^{184}\text{Tl}$ , was 4.9(1)% and 0.76(3)% in Ge1 and Ge2, respectively, for the given geometry. Energy and efficiency calibrations were performed using standard sources of  $^{133}\text{Ba}$ ,  $^{137}\text{Cs}$ ,  $^{60}\text{Co}$ , and  $^{152}\text{Eu}$ . In the detection setup, digital electronics [digital gamma finder (DGF) modules [23]] were used to acquire the data. Unfortunately, due to the high count rates, we suffered from a dead time effect caused by the buffer read-outs of the DGF modules.

## III. INTERNAL DECAY OF THE $(10^-)$ ISOMER

During the experimental campaign, three different data sets were acquired. In the first data set, the thallium atoms were ionized only through surface ionization. A second data set consists of laser scans, where decay spectra were taken as a

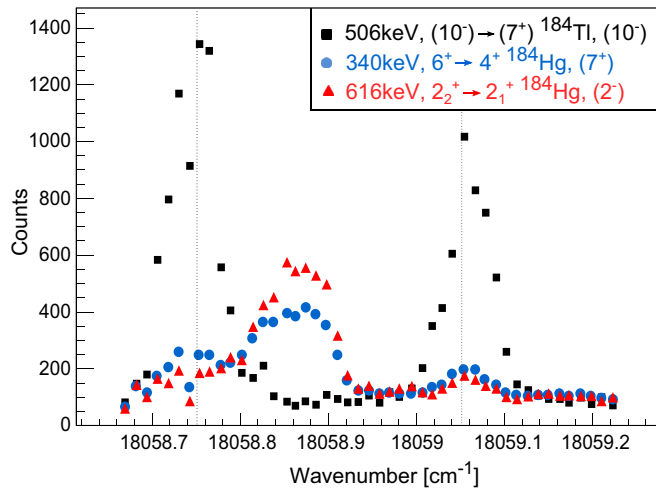


FIG. 1. (Color online) Intensity of the 506 keV (black squares), 340 keV (blue circles), and 616 keV (red triangles)  $\gamma$  lines as a function of the first excitation step laser wave number (before frequency doubling). The origin of the different  $\gamma$  lines is given in the inset and further discussed in the text. The vertical dashed lines indicate the wave number (before frequency doubling) to which the first step narrow band laser was tuned in order to enhance the production of the ( $10^-$ ) state.

function of the first excitation step laser frequency. And then finally a third data set was acquired, where the first excitation step laser frequency was tuned in order to selectively enhance the production of the ( $10^-$ ) state and, through its IT, also the ( $7^+$ ) state relative to the ( $2^-$ ) state. Combining these different data sets we were able to disentangle the decay schemes of the three long-lived states in  $^{184}\text{Tl}$  [20,21], namely, the  $\alpha$  decay and IT of the ( $10^-$ ), the  $\alpha$  and  $\text{EC}/\beta^+$  decay of the ( $7^+$ ) and the ( $2^-$ ).

The presence of different decaying states in  $^{184}\text{Tl}$  can be clearly demonstrated using the intensity as a function of wave number for specific  $\gamma$  lines. Figure 1 shows results from the second data set where the intensity evolution of three such  $\gamma$  rays, each of them specific for the decay from one of the three long-lived states, is given as a function of the wave number of the first excitation step laserlight. Due to the difference in nuclear properties (spin, magnetic moment, charge radius) of the isomers, the atomic levels are splitting and shifting differently through the hyperfine interaction making the laser-ionization efficiency for the different isomers wave number dependent. The 506 keV transition originates purely from the ( $10^-$ ) state in  $^{184}\text{Tl}$  and leads to a hyperfine structure pattern characteristic for the ( $10^-$ ) state. The 340 keV  $\gamma$  line is the  $6^+ \rightarrow 4^+$  transition in  $^{184}\text{Hg}$ . The former is predominantly fed by the ( $7^+$ )  $\beta$  decay in  $^{184}\text{Tl}$  which leads to a hyperfine structure pattern characteristic for the ( $7^+$ ) state. The 616 keV is the  $2_2^+ \rightarrow 2_1^+$  transition in  $^{184}\text{Hg}$ , where the  $2_2^+$  is predominantly fed by the ( $2^-$ )  $\beta$  decay [20]. This leads to a hyperfine structure pattern characteristic for the ( $2^-$ ) state. In the third data set, the wave number (before frequency doubling) of the first step narrow band laser was tuned to  $18058.75 \text{ cm}^{-1}$  or  $18059.05 \text{ cm}^{-1}$ , the maxima for the ( $10^-$ ) state, in order to enhance its production and, through the IT, that of the ( $7^+$ )

state over the ( $2^-$ ) state. These wave numbers are indicated in Fig. 1 by the vertical dashed lines.

Another way to discriminate between the isomers is by making use of the difference in half-life. This is unfortunately not possible for the ( $7^+$ ) and ( $2^-$ ) states as they have similar half-lives ( $T_{1/2} \sim 10 \text{ s}$  [24–26]). However, based on the systematics of the  $[\pi 1h_{9/2} \otimes \nu 1i_{13/2}]$  to  $[\pi 3s_{1/2} \otimes \nu 1i_{13/2}]$  IT in the heavier odd-odd thallium isotopes, a half-life in the order of  $\sim 100 \text{ ms}$  is expected for the ( $10^-$ ) isomer. The pulsed structure of the proton beam together with the short implantation time after each proton pulse enables the discrimination between short- and long-living activity as is shown in Fig. 2. Spectrum 2(a) is a singles  $\gamma$ -ray energy spectrum collected between 10 and 200 ms after each proton pulse and thus contains relatively more short-living than long-living activity. Spectrum 2(b) was acquired starting from 200 ms after each proton pulse until the next proton pulse. Many  $\gamma$  rays are present in both spectra, mostly originating from the  $\beta$  decay of  $^{184}\text{Tl}$  and from longer-lived daughter activities accumulated in the Windmill chamber. Spectrum 2(c) results from the subtraction of spectra 2(a) minus 2(b), after normalization on the 367 keV  $\gamma$  line. The latter is the  $2^+ \rightarrow 0^+$  transition in  $^{184}\text{Hg}$ . The resulting spectrum 2(c) contains only short-living activity. The  $\gamma$  rays indicated with their corresponding energy were attributed to the de-excitation of the ( $10^-$ ) isomeric state.

Before discussing the ( $10^-$ ) decay we will address the peaks and dips indicated with the different symbols in Fig. 2(c). The small peaks at 159 and 198 keV, indicated with a triangle, result from neutron-induced reactions in the surrounding materials. These neutron-induced  $\gamma$  lines have been identified as such since they are already present in the first 5 ms after the proton pulse when the separator beam gate is still closed. Both  $\gamma$  lines are also clearly present in the singles  $\gamma$  spectra of the other thallium isotopes measured during the same experimental campaign. The peak and dips indicated with a full circle originate from a disproportionate subtraction of the long-lived contribution and result in the creation of artificial peaks. However, the origin of the peak at 117 keV, indicated with a square, remains unclear at present.

Using the same procedure used for the singles  $\gamma$ -ray spectra from Fig. 2, an electron spectrum detected with the Si2 detector was constructed. This spectrum (see Fig. 3, open spectrum) contains the IT electrons associated with the decay of ( $10^-$ ) state. The peak at 491 keV corresponds to the  $L, M$ -CE from the 506 keV transition. The  $K$ -CE from the 506 keV and  $L, M$ -CE from the 445 keV transitions give rise to the peak around 421 keV, while the 360 keV peak is attributed to the  $L, M$ -CE from the 374 keV and  $K$ -CE from the 445 keV transitions. The filled spectrum in Fig. 3 represents electrons in coincidence with the  $K_{\alpha 1}$  line from thallium and is collected between 10 and 200 ms after the proton pulse.

In Fig. 4 the time distribution of the events in the 506 keV  $\gamma$  line is shown. The dotted red line shows the result of a fit by an exponential curve with a constant background fixed at ten counts resulting in a half-life value of 47.6(7) ms. A deviation from the fitted curve is observed for times larger than 250 ms and is due to the previously mentioned dead time effect. Different fits with a constant background varying

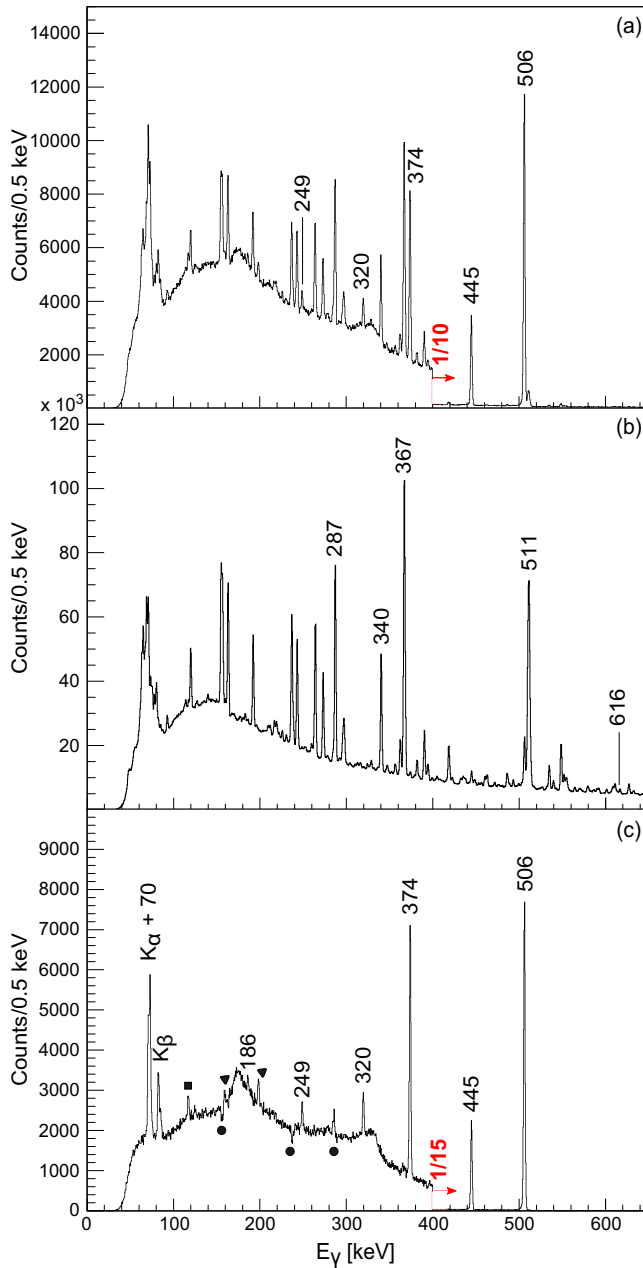


FIG. 2. (Color online)  $\gamma$ -ray singles energy spectra obtained in Ge1 while the first excitation step laser frequency was tuned to enhance the production of the  $(10^-)$  state. Spectrum (a) is spectrum collected between 10 and 200 ms after each proton pulse, enhancing the IT  $\gamma$  rays (the most intense ones are labeled by their energy). Spectrum (b) contains  $\gamma$  rays that were acquired starting from 200 ms after each proton pulse until the next proton pulse, enhancing the  $\gamma$  rays from the  $\beta^+$ /EC decay of  $^{184}\text{Tl}$  (labeled by their energy). Spectrum (c) is a linear combination of the upper two spectra (see text) and contains dominantly the  $\gamma$  lines associated with the decay of the  $(10^-)$  isomeric state. The peaks and dips indicated with different symbols in the spectrum are further discussed in the text.

between 5 and 30 counts were performed. The variation of the resulting half-life values was added as systematic uncertainty to the statistical uncertainty ( $\sigma_{\text{stat}} = 0.3$  ms,  $\sigma_{\text{sys}} = 0.4$  ms). The final half-life value of 47.1(7) ms results from the weighted

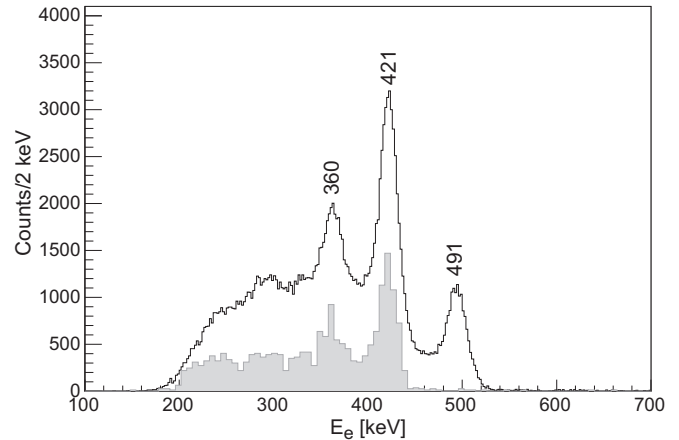


FIG. 3. Electron spectra containing mainly IT activity. The open spectrum was obtained using the same procedure as used to generate spectrum Fig. 2(c). The filled spectrum contains only  $K$ -CE from the decay of the  $(10^-)$  state by applying a coincidence condition on the thallium  $K_{\alpha 1}$  x-rays. It is scaled with an arbitrary factor for visualisation purposes. Electron energies are given in keV.

average of the time behavior of the intensity of the  $\gamma$  lines at 506, 445, and 374 keV, the  $K$ - and  $L$ -CE from the 506 keV transition and the  $\alpha$  line from the decay of the  $(10^-)$  isomer. The  $\alpha$  decay of this isomer, identified for the first time in this study, will be further discussed in Ref. [21].

The decay scheme shown in Fig. 5 is constructed based on the knowledge of previous experiments [8] and all the  $\gamma$  rays assigned to the IT of the  $(10^-)$  state in the singles  $\gamma$ -ray energy spectrum of Fig. 2 and Table I, using the Rydberg-Ritz combination principle [27]. Due to low count rates no  $\gamma$ - $\gamma$  coincidences could be obtained. Spin assignments of the different levels are made based on deduced  $\gamma$ -ray multiplicities. The multiplicities have been attributed by

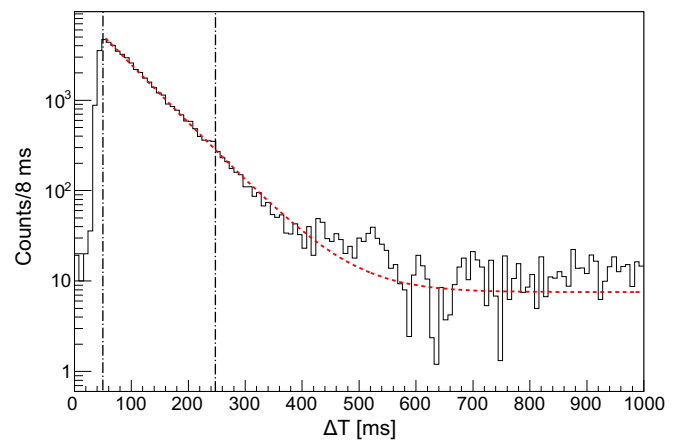


FIG. 4. (Color online) Time distribution of the events in the 506 keV  $\gamma$  line from the  $(10^-)$  isomeric state. The dotted red line shows the result of a fit from 50 to 250 ms by an exponential curve with a constant background fixed at ten counts resulting in the half-life value of 47.6(7) ms. The fit range from 50 to 250 ms is indicated by the vertical dashed lines.

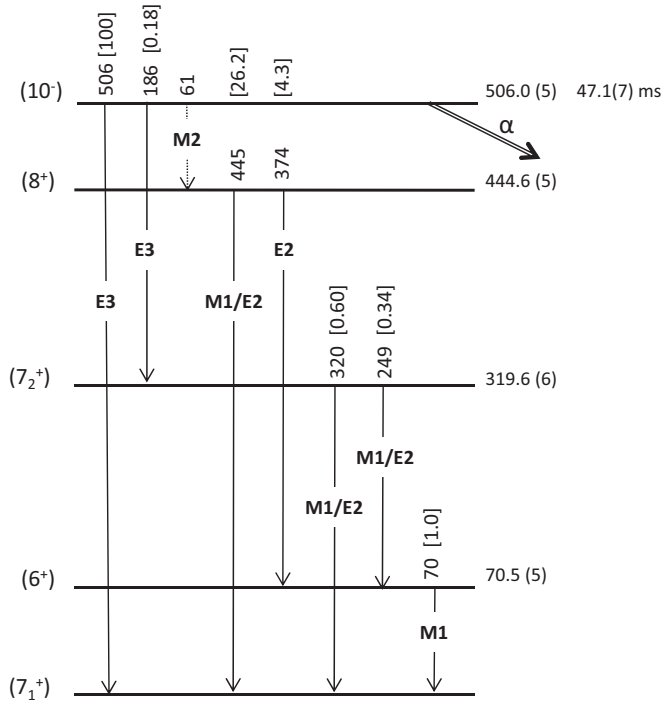


FIG. 5. Decay scheme of the  $(10^-)$  isomer in  $^{184}\text{Tl}$ . The energies of the levels and transitions are in keV. The transition intensities (relative to the 506 keV transition intensity) are given in brackets. The deduced multipolarity of each  $\gamma$  line is indicated on the corresponding transition.

using the  $\gamma$ , electron and  $K$  x-ray intensities and the partial half-life of the transitions, starting from the  $(10^-)$  IT (see Table I). (Note: From analysis of the  $\alpha$  decay of the  $(10^-)$  state, it was deduced that the  $\alpha$ -branching ratio is negligible when determining the partial half-lives of the  $\gamma$  transitions de-exciting the  $(10^-)$  isomeric state [21].) The multipolarity of the 445 keV is deduced by using the intensity of the 360 keV electrons ( $K$  conversion of the 445 keV transition) in the Si2 detector coincident with the thallium  $K_{\alpha_1}$  x-rays in Ge1 (see the filled spectrum in Fig. 3), the intensity of the

TABLE I. Energy, relative intensity and deduced multipolarity for the  $\gamma$  rays observed in the decay of the  $(10^-)$  isomeric state. The relative intensities of  $K_{\alpha_{1,2}}$  and  $K_{\beta_{1,2}}$  x-rays associated with the IT of  $^{184}\text{Tl}$  are also listed.

$E_\gamma$ (keV)	$I_\gamma$ (%)	Deduced multipolarity
506.1 (1)	100	$E3$
444.8 (1)	26.2 (9)	$M1/E2$
373.9 (1)	4.3 (1)	$E2$
319.8 (4)	0.60 (3)	$M1/E2$
248.9 (2)	0.34 (3)	$M1/E2$
186.2 (3)	0.18 (4)	$E3$
70.5 (5)	1.0 (8)	$M1$
$K_{\alpha_{1,2}}$	5.9 (4)	
$K_{\beta_{1,2}}$	1.6 (2)	

TABLE II. Energy and deduced multipolarity and corresponding retardation factor  $F_w$  for  $E3$  and  $M2$  isomeric transitions in  $^{183-188}\text{Tl}$ . Data for  $^{184}\text{Tl}$  are from this work, the other isotopes from [6,38].

Isotope	$E_\gamma$ (keV)	Multipolarity	Retardation factor $F_w$
$^{183}\text{Tl}$	(352)	$E3$	(79(1))
$^{184}\text{Tl}$	506	$E3$	984(38)
$^{184}\text{Tl}$	186	$E3$	486(115)
$^{184}\text{Tl}$	61	$M2$	$3.84 \times 10^4(16)$
$^{185}\text{Tl}$	169	$E3$	119(13)
$^{186}\text{Tl}$	374	$E3$	6470(447)
$^{187}\text{Tl}$	36	$E3$	99(2)
$^{188}\text{Tl}$	269	$M2$	$1.89 \times 10^5(19)$

445 keV  $\gamma$  line in singles and the measured efficiencies in the respective Si and Ge detectors. A  $K$ -conversion coefficient of 0.09(2) is obtained: this excludes an  $E1$  multipolarity ( $\alpha_{CE,K}(\text{theor.}) = 0.00977(14)$  [28]) but leaves the possibility of  $[78^{(+22)}_{-26}\%M1 + 22^{(+26)}_{-22}\%E2]$  or  $[10^{(+16)}_{-10}\%M2 + 90^{(+10)}_{-16}\%E3]$  [28]. However, out of the intensity ratio between the 360 keV electron line and the 421 keV electron line ( $K$  conversion of the 506 keV transition) in the filled spectrum of Fig. 3, only the multipolarity combination  $E3$  for the 506 keV transition ( $\alpha_{CE,K}(\text{theor.}) = 0.0489(7)$  [28]) and  $M1 + E2$  for the 445 keV transition remains. The  $E3$  character of the 506 keV transition is in agreement with the previously proposed spin and parity of the IT isomeric state at 506 keV  $(10^-)$  and the high spin  $\beta$ -decaying state  $(7^+)$  [8]. The 445 keV level is fed in the IT of the  $(10^-)$  isomer by an unobserved thus highly converted, parity-changing 61 keV transition. Attributing a pure  $E3$  character to this 61 keV transition would lead to an unphysically low retardation factor  $F_w$  of 2.7 (1), while a pure  $M2$  transition leads to a reasonable retardation factor  $F_w$  of  $3.84 \times 10^4(16)$  (see Table II for an overview of  $M2$  and  $E3$  retardation factors in the thallium isotopes). Therefore a  $(8^+)$  spin and parity is proposed for the level at 445 keV. The level at 320 keV was previously observed by Andreyev *et al.* [8] through a prompt coincidence between feeding  $\alpha$  lines and the  $\gamma$  rays decaying out of this state, restricting the possible multipolarity of the 320 and 249 keV transitions to  $E1$ ,  $M1$ , and  $E2$ . Both transitions have the same parity as the 70 keV transition, fed by the 249 keV transition and which is of  $M1$  character [8]. In the IT of the  $(10^-)$  isomer, the 320 keV level is fed by the 186 keV transition. Depending on the multipolarity of the 320 and 249 keV transitions, the obtained total conversion coefficient of the 186 keV transition lies between 4.3 and 9.2, allowing  $M2$  and  $E3$  multipolarity but excluding  $M3$ . The preference for an  $E3$  multipolarity assignment for the 186 keV transition is based on the associated retardation factor  $F_w$  of 486(115) which is consistent with other  $E3$  retardation factors in the thallium isotopes (see Table II), while the retardation factor of  $8.5 \times 10^6(20)$  for a  $M2$  transition is rather high. Furthermore, attributing a  $M2$  character to the 186 keV transition would require an unexpected second low-lying  $8^+$  state. Concluding, a  $(7^+)$  spin and parity is preferred for the state at 320 keV. The level at 70 keV was previously observed by Andreyev *et al.* [8]

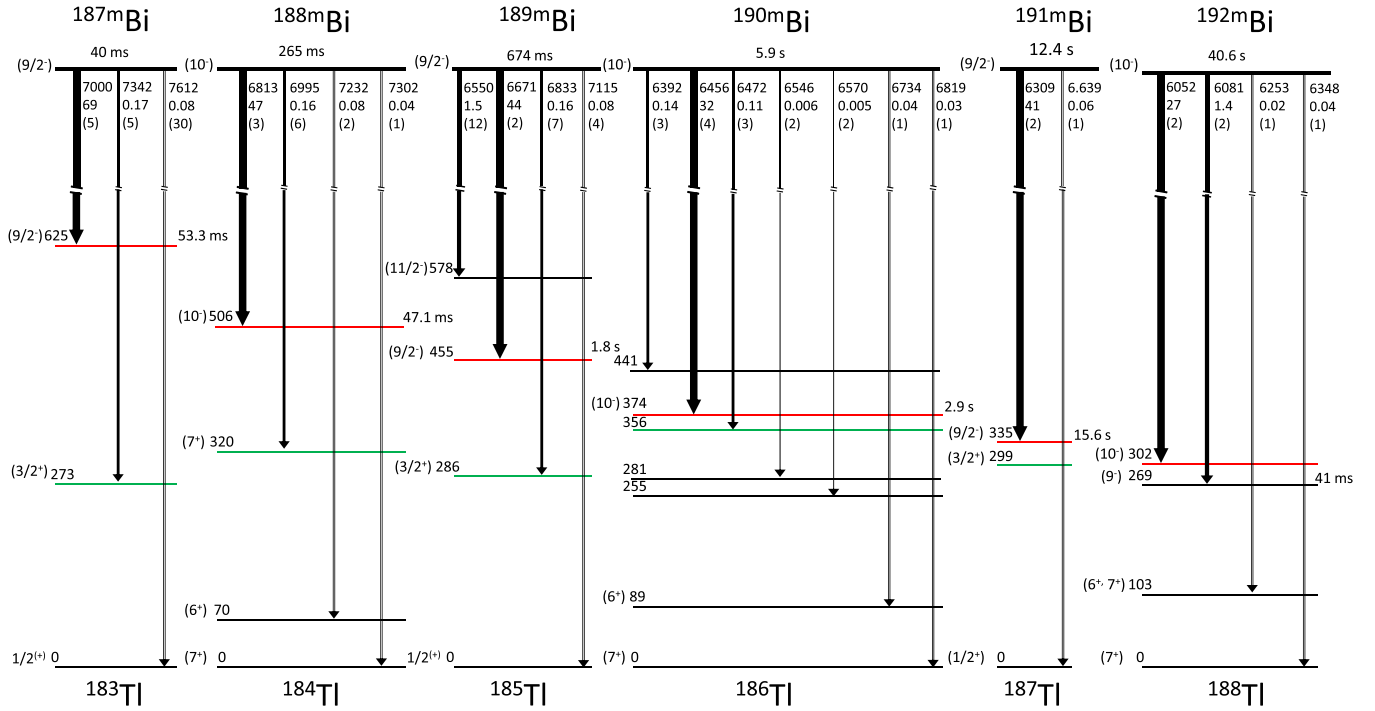


FIG. 6. (Color online)  $\alpha$ -decay information from  $^{192}\text{Bi}$  down to  $^{187}\text{Bi}$  involving the  $1h_{9/2}$  proton configuration. The  $\alpha$ -decay energy and corresponding reduced width (in keV) are indicated next to each transition. The errors on the reduced widths are shown within brackets. All energies are in keV. The states in the daughter thallium isotopes involving the  $\pi 1h_{9/2}$  orbitals are indicated in red, those involving the  $\pi 2d_{3/2}$  in green. The data are taken from [8,31–36].

and a  $M1$  multipolarity was deduced for its de-excitation to the  $(7^+)$   $\beta$ -decaying state. In the  $(10^-)$  decay this level is fed through the 249 and 374 keV transitions. The 1%  $\gamma$ -ray intensity of its depopulating 70 keV  $\gamma$  line is in agreement with the previously measured conversion coefficient of 5(1) [8].

#### IV. DISCUSSION

In the region around neutron midshell at  $N = 104$  low-lying excited states in the even-mass thallium isotopes result mainly from the coupling of the odd proton occupying the normal  $\pi 3s_{1/2}$ ,  $\pi 2d_{3/2}$ , or intruder  $\pi 1h_{9/2}$  orbitals with the odd neutron in the  $\nu 3p_{3/2}$  or  $\nu 1i_{13/2}$  orbitals. All the odd-mass thallium isotopes ranging from  $A = 201$  down to 181 have a  $(1/2^+)$  ground state, a  $(3/2^+)$  excited state between 258 and 386 keV, and a  $(9/2^-)$  intruder state showing a distinct parabolic behavior of the excitation energy as a function of neutron number reaching its minimum at  $N = 108$ . The allocation of the states in the odd-odd thallium isotopes within each full multiplet will primarily depend on the specific proton-neutron residual interaction in these  $[j_p \otimes j_n]J^\pi$  configurations. This has been thoroughly discussed by several authors [6,29–32]. The two lowest states in Fig. 5,  $(7_1^+)$  and  $(6^+)$ , have been proposed in Ref. [8] as two members of the  $[\pi 3s_{1/2} \otimes \nu 1i_{13/2}]_{6^+,7^+}$  multiplet of states, while the  $(10^-)$  is associated with the intruder based  $[\pi 1h_{9/2} \otimes \nu 1i_{13/2}]_{2^- \rightarrow 11^-}$  configuration. In the present work the levels at 320 [8] and 445 keV have been tentatively assigned spin and parity  $(7^+)$  and  $(8^+)$ , respectively. Both are candidates for members of the  $[\pi 2d_{3/2} \otimes \nu 1i_{13/2}]_{5^+ \rightarrow 8^+}$  multiplet. Their energy fits well in

the systematics presented in Fig. 6, where the position of the  $(3/2^+)$   $[\pi 2d_{3/2}]$  level in the neighboring odd-mass thallium isotopes is given. In  $^{186}\text{Tl}$  [8] the levels at 255, 281, 356, and 441 keV were also attributed to the  $[\pi 2d_{3/2} \otimes \nu 1i_{13/2}]_{5^+ \rightarrow 8^+}$  multiplet, although the possibility was left open that the 356 and 441 keV levels are originating as, respectively, the  $5^-$  and  $(6, 7, 8, 9 \text{ or } 11)^-$  members from the  $[\pi 1h_{9/2} \otimes \nu 1i_{13/2}]_{2^- \rightarrow 11^-}$  multiplet.

Next to energy systematics, information on the underlying structure of the different isotopes can be obtained through the reduced widths of the  $\alpha$  transitions feeding the levels and through the transition probabilities of the electromagnetic radiation feeding and de-exciting the levels. The  $\alpha$  decay of bismuth towards thallium is crossing the  $Z = 82$  closed shell and in principle only hindered  $\alpha$  decay is expected as the proton configurations are very different. However, allowed  $\alpha$  decay is observed and this was used to characterize proton intruder states in the bismuth mother and thallium daughter, see [7,8,33] (and references therein). In Fig. 6 the  $\alpha$ -decay information from  $^{192}\text{Bi}$  down to  $^{187}\text{Bi}$  involving the  $1h_{9/2}$  proton configuration is presented. This is the decay from the  $(9/2^-)$  state for the odd-mass bismuth isotopes and the decay from the  $(10^-)$   $[\pi 1h_{9/2} \otimes \nu 1i_{13/2}]$  state for the even-mass bismuth isotopes. The reduced widths for  $\alpha$  decay have been calculated using the Rasmussen formalism [37]. Five classes of reduced widths can be observed: 20–70 keV,  $\sim 1.5$  keV,  $\sim 0.16$  keV, 0.02–0.08 keV, and  $\sim 0.005$  keV. In this mass region, allowed  $\alpha$  decay in even-even nuclei typically has reduced widths between 30 and 60 keV. In  $^{187-192}\text{Bi}$ ,  $\alpha$ -decay transitions between two states with equal spin and parity are

observed with reduced widths varying between 27 and 69 keV (see Fig. 6). The ( $9/2^-$ )  $\rightarrow$  ( $11/2^-$ ) decay and ( $10^-$ )  $\rightarrow$  ( $9^-$ ) decays have a reduced width around 1.5 keV. The decay towards the  $\pi 2d_{3/2}$  state in the odd thallium isotopes has a reduced width around 0.16 keV. In  $^{188}\text{Bi}$  a transition with a similar reduced width feeds respectively a level at 320 keV. In  $^{190}\text{Bi}$  two levels receive similar feeding: the level at 356 keV and at 441 keV. Based on this and their energy position, it is tempting to interpret these levels as originating from the proton  $\pi 2d_{3/2}$  configuration coupled to the  $1i_{13/2}$  neutron. The decay involving the  $\pi 1h_{9/2}$  configuration in the odd-mass bismuth isotopes and the  $\pi 3s_{1/2}$  configuration in the thallium daughters is strongly hindered and the reduced widths lie between 0.02 and 0.08 keV. In the even-mass bismuth decay transitions hindered with the same order of magnitude are feeding the lowest ( $6^+$ ) and ( $7^+$ ) levels. Based on the same arguments developed above, these levels are interpreted as originating from the  $\pi 3s_{1/2}$  proton coupled to the  $1i_{13/2}$  neutron. In  $^{186}\text{Tl}$  the levels at 255 and 281 keV are even one order of magnitude less fed and the increased hindrance, around 0.005 keV, is discussed in terms of the angular-momentum coupling between the  $[\pi 2d_{3/2} \otimes \nu 1i_{13/2}]$  [8]. Unfortunately it was not possible in Ref. [8] to observe similar states in  $^{184}\text{Tl}$  due to the limited statistics. Also in the present study no extra levels around 300 keV were observed possibly owing to the specific decay path of the ( $10^-$ ) isomeric decay bypassing these levels.

In addition to the  $\alpha$ -decay reduced widths the deduced  $\gamma$ -ray transition probabilities between normal and intruder states can give further insight in the underlying nuclear configuration. The retardation factors  $F_w$ , the rate of a transition compared to the Weiskopf estimate, of the isomeric  $E3$  and  $M2$  transitions in odd and even mass thallium isotopes are listed in Table II. In the odd-mass thallium isotopes retardation factors for the ( $9/2^-$ ) to ( $3/2^+$ )  $E3$  transition in the order of 100 are observed. This retardation is related to the configuration change of the proton from the  $1h_{9/2}$  to the  $2d_{3/2}$  orbital ( $\Delta\ell = 3$ ). The retardation of the  $E3$  transition in the odd-odd  $^{186}\text{Tl}$  [6] is however significantly higher. This increase in hindrance factor can be related to the different nature of the stretched  $E3$  transition as it involves configuration changes from a  $[\pi 1h_{9/2} \otimes \nu 1i_{13/2}]$  to a  $[\pi 1s_{1/2} \otimes \nu 1i_{13/2}]$  ( $\Delta\ell = 5$ ). In  $^{184}\text{Tl}$  the retardation of the transition from the intruder-based ( $10^-$ ) state to the ( $7_1^+$ ) state is about seven times smaller than the equivalent transition in  $^{186}\text{Tl}$ . This possibly hints towards increased mixing of the  $[\pi 2d_{3/2} \otimes \nu 1i_{13/2}]$  configuration in

the ( $7_1^+$ ) state. Moreover, the ( $10^-$ )  $\rightarrow$  ( $7_2^+$ )  $E3$  transition being twice as fast as the ( $10^-$ )  $\rightarrow$  ( $7_1^+$ ) transition points also to a larger  $[\pi 2d_{3/2} \otimes \nu 1i_{13/2}]$  content in the ( $7_2^+$ ) state compared to that in the ( $7_1^+$ ). It is interesting to note that also in the hyperfine structure measurements in the same experiment, the  $g$  factor of the ( $7_1^+$ ) state shows increased importance of the  $[\pi 2d_{3/2} \otimes \nu 1i_{13/2}]$  configuration, compared to respective  $g$  factors in the heavier odd-odd thallium isotopes [5,39].

## V. CONCLUSION

The decay of the ( $10^-$ ) isomeric state in  $^{184}\text{Tl}$  was studied at the ISOLDE facility. The half-life was deduced as  $T_{1/2} = 47.1(7)$  ms and its IT decay measured. The precisely determined excitation energy of this state [506.1(1) keV] extends the ( $10^-$ )  $\rightarrow$  ( $7^+$ ) energy systematics beyond neutron midshell and confirms the parabolic behavior as a function of neutron number. From the half-life value and branching ratios, the retardation factors of the depopulating  $E3$  and  $M2$  transitions were determined and compared with retardation factors in neighboring odd-mass and even-mass thallium isotopes. Combined with the information on the published reduced widths of the  $\alpha$  decay of  $^{187-192}\text{Bi}$  populating levels in daughter nuclei  $^{183-188}\text{Tl}$ , a confirmation of the proton 1p-2h intruder character of the ( $10^-$ ) isomer and an interpretation of the levels in  $^{184}\text{Tl}$  fed in the isomeric decay in terms of  $[\pi 3s_{1/2} \otimes \nu 1i_{13/2}]$  and  $[\pi d_{3/2} \otimes \nu 1i_{13/2}]$  could be obtained.

It is worth noting that the proton intruder interpretation of the ( $10^-$ ) isomer is supported by the results of the isotopic shift/hyperfine structure measurements in the same experiment [39].

## ACKNOWLEDGMENTS

This work has been funded by FWO-Vlaanderen (Belgium), by GOA/2010/010 (BOF KU Leuven), by the Interuniversity Attraction Poles Programme initiated by the Belgian Science Policy Office (BriX network P7/12), by the European Commission within the Seventh Framework Programme through I3-ENSAR (contract no. RII3-CT-2010-262010), by a grant from the European Research Council (ERC-2011-AdG-291561-HELIOS), by a grant from the U.K. Science and Technology Facilities Council, by the Slovak Research and Development Agency under Contract No. APVV-0177-11, and by Slovak grant agency VEGA (contract no. 2/0121/14).

[1] K. Heyde *et al.*, *Phys. Rep.* **102**, 291 (1983), and references therein.  
 [2] J. L. Wood *et al.*, *Phys. Rep.* **215**, 101 (1992), and references therein.  
 [3] R. Julin *et al.*, *J. Phys. G: Nucl. Part. Phys.* **27**, R109 (2001), and references therein.  
 [4] K. Heyde and J. L. Wood, *Rev. Mod. Phys.* **83**, 1467 (2011), and references therein.  
 [5] A. E. Barzakh *et al.*, *Phys. Rev. C* **88**, 024315 (2013), and references therein.

[6] A. J. Kreiner, C. Baktash, G. Garcia Bermudez, and M. A. J. Mariscotti, *Phys. Rev. Lett.* **47**, 1709 (1981).  
 [7] A. N. Andreyev *et al.*, *Eur. Phys. J. A* **18**, 55 (2003).  
 [8] A. N. Andreyev *et al.*, *Eur. Phys. J. A* **18**, 39 (2003).  
 [9] C. Bohm *et al.*, *Phys. Rev. C* **90**, 044307 (2014).  
 [10] V. N. Fedoseev *et al.*, *Hyperfine Interact.* **127**, 409 (2000).  
 [11] V. N. Fedoseev *et al.*, *Rev. Sci. Instrum.* **83**, 02A903 (2012).  
 [12] V. N. Fedoseev, Y. Kudryavtsev, and V. I. Mishin, *Phys. Scr.* **85**, 058104 (2012).

- [13] G. D. Alkhazov *et al.*, *Nucl. Instrum. Methods Phys. Res. B* **69**, 517 (1992).
- [14] A. E. Barzakh *et al.*, *Eur. Phys. J. A* **1**, 3 (1998).
- [15] V. N. Fedoseev *et al.*, *Nucl. Instrum. Methods Phys. Res. B* **204**, 353 (2003).
- [16] E. Kugler, *Hyperfine Interact.* **129**, 23 (2000).
- [17] A. N. Andreyev *et al.*, *Phys. Rev. Lett.* **105**, 252502 (2010).
- [18] J. Elseviers *et al.*, *Phys. Rev. C* **88**, 044321 (2013).
- [19] M. Seliverstov *et al.*, *Phys. Rev. C* **89**, 034323 (2014).
- [20] E. Rapisarda *et al.* (unpublished).
- [21] C. Van Beveren *et al.* (unpublished).
- [22] B. Lommel *et al.*, *Nucl. Instrum. Methods Phys. Res. A* **480**, 199 (2002).
- [23] X-ray instruments Associates, <http://www.xia.com> (2010).
- [24] K. S. Toth *et al.*, *Phys. Lett. B* **63**, 150 (1976).
- [25] J. P. Cole *et al.*, *Phys. Rev. Lett.* **37**, 1185 (1976).
- [26] V. A. Bolshakov *et al.*, *Proceedings of the 6th Conference on Nuclei Far from Stability, 9th International Conference on Atomic Masses and Fundamental Constants, Bernkastel-Kues*, IOP Conf. Proc. 132, (IOP, London, 1993), p. 743.
- [27] W. Ritz, *Astrophys. J.* **28**, 237 (1908).
- [28] <http://bricc.anu.edu.au/>.
- [29] J. Van Maldeghem and K. Heyde, *Fizika* **22**, 233 (1990).
- [30] A. J. Kreiner, *Z. Phys. A* **288**, 373 (1978).
- [31] M. Huyse *et al.*, *Phys. Lett. B* **201**, 293 (1988).
- [32] P. Van Duppen *et al.*, *Nucl. Phys. A* **529**, 268 (1991).
- [33] E. Coenen, K. Deneffe, M. Huyse, P. Van Duppen, and J. L. Wood, *Phys. Rev. Lett.* **54**, 1783 (1985).
- [34] A. N. Andreyev *et al.*, *Phys. Rev. C* **73**, 044324 (2006).
- [35] A. N. Andreyev *et al.*, *Eur. Phys. J. A* **6**, 381 (1999).
- [36] J. C. Batchelder *et al.*, *Eur. Phys. J. A* **5**, 49 (1999).
- [37] J. O. Rasmussen, *Phys. Rev.* **113**, 1593 (1959).
- [38] A. G. Schmidt *et al.*, *Phys. Lett. B* **66**, 133 (1977).
- [39] A. E. Barzakh *et al.* (unpublished).